Journal of Magnetic Resonance 192 (2008) 269–274

Contents lists available at ScienceDirect

Journal of Magnetic Resonance

journal homepage: www.elsevier.com/locate/jmr

Estimation of mean and median pO_2 values for a composite EPR spectrum

Rizwan Ahmad [a], Deepti S. Vikram [a], Lee C. Potter [b], Periannan Kuppusamy [a,*]

[a] Center for Biomedical EPR Spectroscopy and Imaging, Davis Heart and Lung Research Institute, Department of Internal Medicine, The Ohio State University, 420 West 12th Avenue, TMRF-114, Columbus, OH 43210, USA
[b] Department of Electrical and Computer Engineering, The Ohio State University, Columbus, OH 43210, USA

ARTICLE INFO

Article history:
Received 17 December 2007
Revised 26 February 2008
Available online 10 March 2008

Keywords:
EPR spectroscopy
Oximetry

ABSTRACT

Electron paramagnetic resonance (EPR)-based oximetry is capable of quantifying oxygen content in samples. However, for a heterogeneous environment with multiple pO_2 values, peak-to-peak linewidth of the composite EPR lineshape does not provide a reliable estimate of the overall pO_2 in the sample. The estimate, depending on the heterogeneity, can be severely biased towards narrow components. To address this issue, we suggest a postprocessing method to recover the linewidth histogram which can be used in estimating meaningful parameters, such as the mean and median pO_2 values. This information, although not as comprehensive as obtained by EPR spectral–spatial imaging, goes beyond what can be generally achieved with conventional EPR spectroscopy. Substantially shorter acquisition times, in comparison to EPR imaging, may prompt its use in clinically relevant models. For validation, simulation and EPR experiment data are presented.

1. Introduction

The ability of EPR oximetry [1–4] to make repeated, minimally invasive, and locally specific measurements of concentration or partial pressure of oxygen (pO_2) over time can provide vital information to characterize the progression of a disease state, or determine the efficacy of different treatment options. For instance, in tumors, oxygen concentration is considered to be an important factor for determining the response of tumors to various treatment options [5]. Likewise, the presence of oxygen plays a critical role in the pathophysiology of myocardial injury during both ischemia and subsequent reperfusion [6]. Unfortunately, the long data acquisition times, especially for EPR imaging (EPRI), have curtailed wider use of EPR for such important biological applications. EPR spectroscopy, while readily performed for many applications, does not report an accurate measure of pO_2 value for a heterogeneous environment, such as a tumor, where pO_2 distribution is spatially heterogeneous. In this paper, we present a method to recover the linewidth histogram which provides the relative spin densities associated with various linewidths (pO_2) present in the sample. This histogram can be used to extract meaningful information, such as mean and median pO_2 values, without performing the time-consuming spectral–spatial imaging. This method is not a substitute for spectral–spatial imaging since so spatial information is inferred from the data.

In traditional continuous wave EPR (CW-EPR) spectroscopy, the first derivative of absorption spectrum is collected by sweeping the magnetic field in the presence of radio frequency or microwave excitation. The linewidth for oxygen sensitive EPR probes [7] can be readily computed by measuring the peak-to-peak width of the lineshape. If pO_2 is homogeneous over the area of measurement, the information of peak-to-peak linewidth is adequate to estimate the true pO_2 value. However, for a heterogeneous environment, where different locations possess different pO_2 values, the peak-to-peak linewidth of the composite spectrum does not provide an accurate measure of the overall pO_2. Further, EPR spectroscopy does not provide any information regarding the spatial location of spins because the measured spectrum is a sum of spectra from all irradiated sample locations. EPR imaging (EPRI), on the other hand, provides the spin density of the EPR sensitive probe at various spatial locations under the assumption that the spectral lineshape is spatially invariant. For imaging, the main magnetic field is swept in the presence of a magnetic field gradient, and the process is repeated for different gradient orientations to encode the spatial information as Radon projections. For a heterogeneous environment, where lineshape varies with spatial location, an additional dimension called spectral dimension is considered to map both the spatial location of spins and their lineshape. This mode of imaging is called spectral–spatial or spectroscopic imaging [8]. Despite all technological advances, EPR-based imaging, especially the spectral–spatial imaging, is a time-consuming process. For example, more than a thousand projections, each taking two or more seconds, may be required for traditional 4D spectral–spatial imaging.

* Corresponding author. Fax: +1 614 292 8454.
E-mail address: kuppusamy.1@osu.edu (P. Kuppusamy).

1090-7807/$ - see front matter © 2008 Elsevier Inc. All rights reserved.
doi:10.1016/j.jmr.2008.03.002

Recently, Grinberg et al. suggested a method [9] to reduce the dimensionality of the spectral–spatial imaging by implanting particulate probes in the object such that all implants are spatially well-separated for some gradient orientation. Hence, by collecting two projections along that orientation, each with a different gradient strength, the pO_2 values at various spatial locations can be estimated using a convolution-based fitting method. The requirements of well-organized probe distribution, however, may become stringent for many EPR applications where the distribution cannot be confined to few well-separated spots or the user does not have a precise control over the distribution of the probe.

Regression analysis of composite EPR spectra, for a small number of components, has been briefly addressed by Williams et al. [10]. In this paper, we provide a more comprehensive treatment of the subject. Our method is valid for infinitely many components. First, we reformulate this regression problem in the form of a linear operator acting upon the linewidth histogram to be estimated. Second, we compute the minimum-norm constrained least-squares solution to estimate the linewidth histogram. Third, we calculate the mean and median linewidth values from the estimated histogram. The method is robust against realistic noise levels and is flexible enough to accommodate effects of dispersion signal contributions and baseline drift. Simulation and experimental results are provided for verification.

2. Theory

The data collection for EPR spectroscopy can be expressed as

$$b(B) = \int_{\gamma=\gamma_{\min}}^{\gamma_{\max}} x(\gamma)a(B,\gamma)\,\mathrm{d}\gamma \tag{1}$$

where B is the main magnetic field magnitude, $a(B,\gamma)$ is the lineshape that depends on full-width at half-maximum (FWHM) linewidth parameter γ, $x(\gamma)$ is the input histogram that reflects the true relative spin densities associated with various components, and $[\gamma_{\min},\gamma_{\max}]$ is the range of linewidths present in the sample, which depends on the intrinsic linewidth of the probe and the range of pO_2 values present in the sample. For most EPR oximetry probes, the lineshape $a(B,\gamma)$ collected on a conventional CW-EPR spectrometer is the first derivative of Lorentzian function, given by

$$a(B,\gamma) = \frac{-16}{\pi}\,\frac{(B-B_0)\gamma}{(4(B-B_0)^2+\gamma^2)^2} \tag{2}$$

where B_0 is the magnetic field value at resonance which is assumed to be identical for all lineshapes. The lineshape given in Eq. (2) is normalized, i.e., the corresponding Lorentzian function area, which corresponds to spin density, is unity.

The problem of decomposing the composite spectrum is equivalent to estimating $x(\gamma)$. Once $x(\gamma)$ is calculated, the mean and median pO_2 values can be readily computed. As demonstrated below, the values are more accurate than those based on the peak-to-peak linewidth, which are generally biased towards narrower lineshapes. For instance, Fig. 1 shows that the summation of two first derivative Lorentzian functions, with equal absorption areas (spin densities) but different linewidths, yields a spectrum with apparent linewidth that is much closer to the narrower component. In this paper, apparent linewidth refers to $\sqrt{3}$ times the peak-to-peak linewidth. Therefore, for a pure Lorentzian function, the apparent linewidth refers to FWHM linewidth.

2.1. Problem formulation

In the presence of noise, the measurement process for EPR spectroscopy can be expressed as

$$\langle a(B_i,\gamma), x(\gamma)\rangle + \epsilon = b_i \tag{3}$$

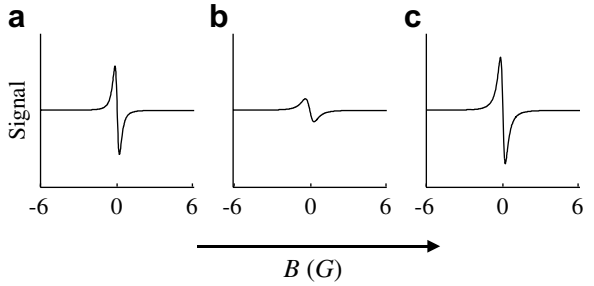

Fig. 1. First derivative Lorentzians (a) FWHM linewidth = 0.6 G, (b) FWHM linewidth = 1.2 G, and (c) their superposition which has apparent linewidth of 0.67 G. Spectra in (a) and (b) represent same spin density.

where ϵ is zero-mean white Gaussian noise with the variance of σ^2, and $\langle\cdot,\cdot\rangle$represents the inner product. Both $a(B_i,\gamma)$ and $x(\gamma)$ are assumed to be elements of the Hilbert space $\mathcal{S}$ of square integrable functions of a single real variable. In terms of the operator A we can rewrite Eq. (3) as

$$Ax + \epsilon = b \tag{4}$$

where $b \in \mathbb{R}^n$ is the list of n measured samples of the EPR spectrum, and $x \in \mathbb{R}^m$ is the unknown spin density histogram to be recovered. For numerical computation, the operator A is implemented by finely sampled discretization of B and γ. The variable B was discretized into $n = 1024$ equally spaced points, consistent with the data sampling used for the L-band spectrometer. The linewidth variable γ was discretized into $m = 512$ equally spaced points on the interval $[\gamma_{\text{low}},\gamma_{\text{up}}]$. From simulation we observed that any finer sampling of these variables did not result in any noticeable improvement in the results.

2.2. Constrained least-squares solution

We can solve Eq. (4) by finding a least-squares solution, which is the minimizer of

$$\min_x \|Ax-b\|^2 \tag{5}$$

Nonnegativity and any other prior constraint on x are expressed by requiring that x belongs to a set $\mathcal{K}$ of admissible solutions. The set $\mathcal{K}$ is assumed to be convex and closed subset of $\mathcal{S}$. Therefore, x can be estimated by solving a constrained least-squares [11] problem

$$\min_x \|Ax-b\|^2 \quad \text{subject to } x \in \mathcal{K} \tag{6}$$

where $\|\cdot\|$ is ℓ_2 norm. Among all the solutions consistent with measurements b and the constraints set $\mathcal{K}$, a minimum-norm solution is of particular interest because it ensures that the contributions for the null space of A are minimized. Because Eq. (6) is an ill-posed problem in general, combating noise sensitivity is another important consideration and is generally accounted for by adding a regularizing term to Eq. (6). Tikhonov regularization, also known as ridge regression, is the most commonly used method for regularizing ill-posed problems [12]. It is a unique minimizer of

$$\min_x \|Ax-b\|^2 + \lambda\|x\|^2 \quad \text{subject to } x \in \mathcal{K} \tag{7}$$

To find a minimum-norm least-squares solution, we adopt an iterative method given in Ref. [13]. Let $P_{\mathcal{K}}$ denote the nonlinear nearest-point projection operator onto the constraint set, $\mathcal{K}$. Then, the minimum-norm least-squares solution, $\hat{x}$, is given by

$$\hat{x} = P_{\mathcal{K}}(A^*\hat{y}) \tag{8}$$

where $\hat{y}$ provides an n-dimensional parameterization for the solution $\hat{x}$, and A^* is the adjoint of A. The parameter vector is found via the convergent iteration

$$y_{k+1} = \beta_k[y_k + \mu_k(b - AP_{\mathcal{K}}(A^* y_k))] \quad (9)$$

where $\beta_k = 1/(1 + \lambda\mu_k)$ controls the contributions from the regularizing term, and μ_k controls the convergence. For our application, $P_{\mathcal{K}}$ is implemented by setting to zero those values of x which are either negative or lie outside of $[\gamma_{\min}, \gamma_{\max}]$. Since $[\gamma_{\min}, \gamma_{\max}]$ may not be precisely known in advance, a wider range $[\gamma_{\text{low}}, \gamma_{\text{up}}]$ that encompasses $[\gamma_{\min}, \gamma_{\max}]$ can be considered.

The optimal regularization parameter λ is usually unknown and often in practice is determined by an ad hoc method. The commonly used approaches include the discrepancy principle, cross-validation, and L-curve method [14]. In our application, we have observed that the minimum-norm constrained least-squares solution is smooth and stable for a wide range of σ^2 and input histograms x. Therefore, no regularization was used ($\beta_k = 1$). To improve convergence, we adopted $\mu_k = c(1 - \cos(k\pi/N))$ with N being the maximum number of iterations and $c \in (0, 2\|A\|^{-2})$. We selected $N = 2500$. The iteration process was terminated when k reached N or when $\|r\|^2 < n\sigma^2$, with $r = A\hat{x} - b$ being the residual.

Undesired contributions from the dispersion signal and baseline drift can alter the lineshape. Fortunately, the dispersion component, which is orthogonal to the absorption component, has zero contributions to the least-squares solution because $A^*b = 0$. Hence, the solution $\hat{x}$ is not affected by the dispersion component and no modification is required in the problem formulation or its implementation. To account for a linear baseline drift, a vector $[-n/2, \ldots n/2]^T$ can be appended to A after discretization.

For additive white Gaussian noise, the constrained least-squares solution $\hat{x}$ provides the maximum likelihood estimate of the histogram x. By the maximum likelihood invariance principle [15], statistics such as mean and median computed from $\hat{x}$ are likewise maximum likelihood estimates. The lineshapes for many EPR oximetry probes may not belong to Lorentzian or any other parametric family of functions [16]. In such cases, the lineshape and its variation with pO_2 can be determined experimentally. Once the lineshape is measured in small increments over the desired range of pO_2 values, the matrix equivalent of A can be readily constructed.

Our analysis of the composite spectrum is suited for a spectrum which has many components. For problems where the composite spectrum is known to be composed of few components, for example, for a model with two point implants in a mouse or rat heart, a more accurate estimation of x can be found by parameterizing the problem in terms of unknown spin densities and linewidths.

3. Results

In this section, we compare the mean and median computed from the reconstructed histogram $\hat{x}$ with the ground truth x for both simulation and L-band spectroscopy experiment.

3.1. Simulation

The composite spectrum was generated by summing 50 first derivative Lorentzian lineshapes with different linewidths, equally spaced in the range of 0.52–3.12 G. The linewidth histogram x was generated by adding two Gaussian histograms each with a standard deviation of 1 G and means that belong to $U[0.52, 1.82]$ and $U[1.82, 3.12]$, respectively. Here, $U[u_1, u_2]$ denoting a uniform probability distribution between u_1 and u_2. The net histogram was normalized to have a maximum of 1. The total sweep width was 12 G, and there were 1024 points in the measured vector b. A zero-mean white Gaussian noise was added to b to maintain a signal-to-noise ratio (SNR) of 12 dB.

We generated 50 different b each having a different linewidth histogram and noise realization. Starting from $x_0 = 0$, the estimated $\hat{x}$ was computed using the proposed method with $[\gamma_{\text{low}}, \gamma_{\text{up}}]$ selected to be $[0.48, 3.20]$. Shown in Figs. 2 and 3 are true and estimated histograms for 2 of the 50 runs considered. Also, note that the error variance for an estimated histogram will be higher for components with larger linewidths [20] because of their lower SNR. This effect is observed in (Fig. 4). The mean and median intensities, computed from both true and estimated histogram for all the 50 runs, are shown in Fig. 5.

3.2. Experiment

A phantom using 50 μL capillary tubes was constructed. Each capillary tube was filled with lithium octa-*n*-butoxy naphthalocyanine (LiNc-BuO) [17] up to a height of 5 mm. Variations in linewidths were obtained by using different amounts of sodium hydrosulfite and water, a combination known for changing the oxygen concentration [18] to which the sample will be exposed. A total of 17 capillary tubes were prepared with FWHM linewidths

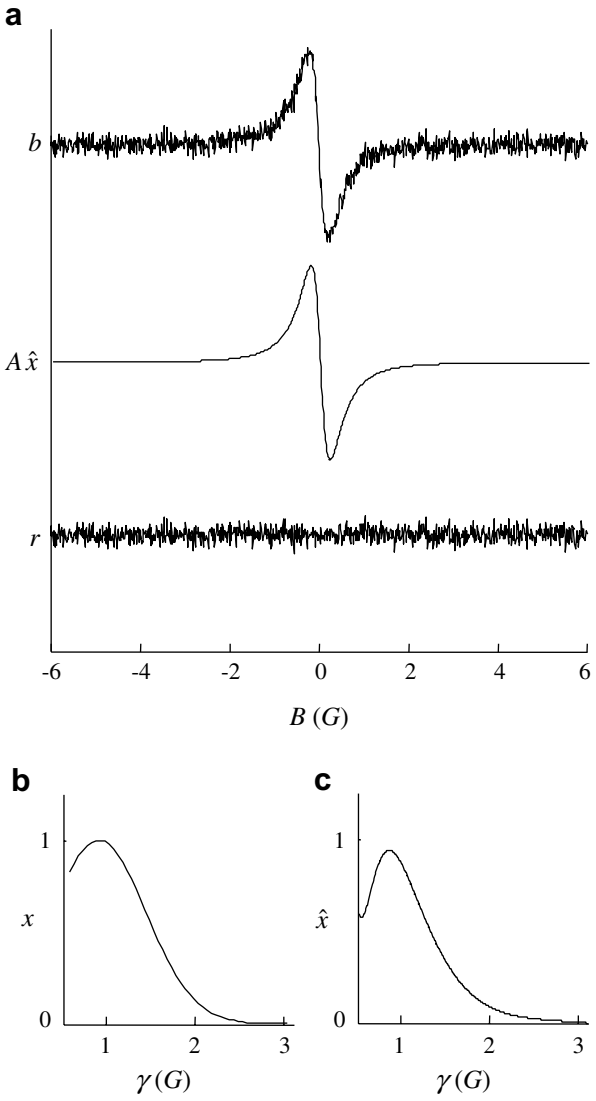

Fig. 2. An example of simulation results. (a) Measured data b, fitting results $A\hat{x}$, and residual r, (b) input histogram x, and (c) estimated histogram $\hat{x}$. Mean linewidths for x and $\hat{x}$ are 0.971 and 0.957 G, while median linewidths for x and $\hat{x}$ are 1.05 and 1.01 G, respectively. Apparent linewidth computed from $A\hat{x}$ is 0.751 G.

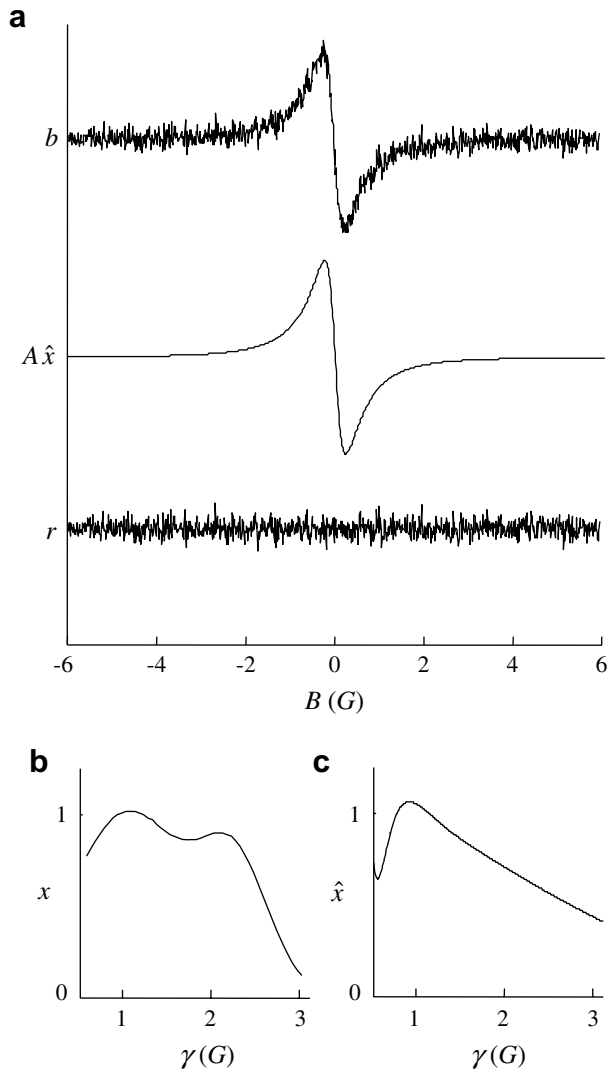

Fig. 3. Another example of simulation results. (a) Measured data b, fitting results $A\hat{x}$, and residual r, (b) input histogram x, and (c) estimated histogram $\hat{x}$. Mean linewidths for x and $\hat{x}$ are 1.31 and 1.32 G, while median linewidths for x and $\hat{x}$ are 1.58 and 1.57 G, respectively. Apparent linewidth computed from $A\hat{x}$ is 0.832 G.

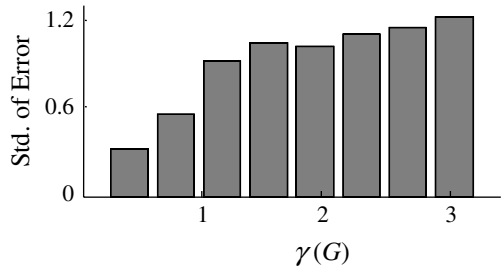

Fig. 4. Standard deviation of error as a function of γ for 50 runs considered.

of {0.63, 0.65, 0.76, 0.83, 1.49, 1.55, 1.64, 1.79, 2.01, 2.48, 2.59, 2.60, 2.83, 2.87, 2.99, 3.27, 3.33}. An L-band (1.2 GHz) EPR system was used for data acquisition. A volume resonator with diameter 12.6 mm and sensitive height 12 mm was used. Spectrometer settings were: incident microwave power of 220 μW, center field of 458.41 G, sweep width of 12 G, time constant of 0.01 s, modulation amplitude of 0.07 G, and scan time of 3.93 s.

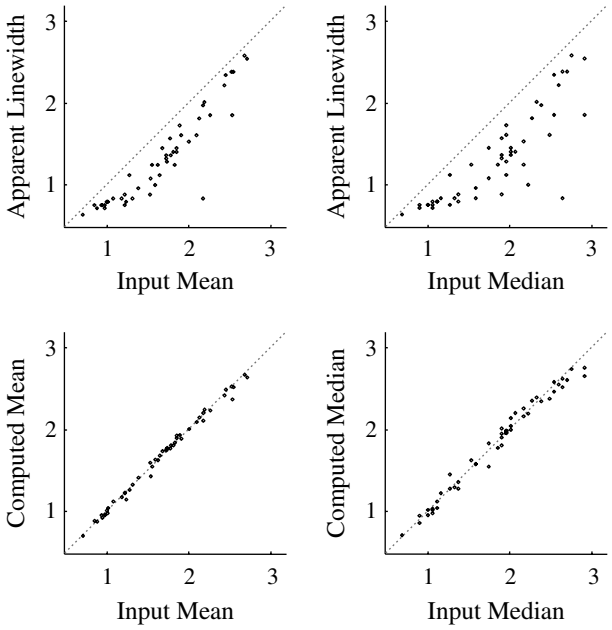

Fig. 5. Mean and median linewidth values, in Gauss, from the input histogram are compared with the peak-to-peak apparent linewidth (top row) and with the mean and median values computed from the estimated histogram (bottom row).

A plastic holder, shown in Fig. 6, was machined to hold the capillary tubes inside the resonator. The data collection included performing EPR spectroscopy for each of the 17 capillary tubes individually to determine their linewidth as well as the relative spin densities, serving as the ground truth. Then, three different combinations of 12–14 capillary tubes were used to generate three different composite spectra named b_1, b_2, and b_3. For each composite spectrum two SNR values, 12 or 24 dB, were considered by changing the receiver gain of the spectrometer. The minimum linewidth present in the sample was 0.63 G while the maximum was 3.33 G. We selected $[\gamma_{low}, \gamma_{up}]$ to be [0.60, 3.5]. The experimental

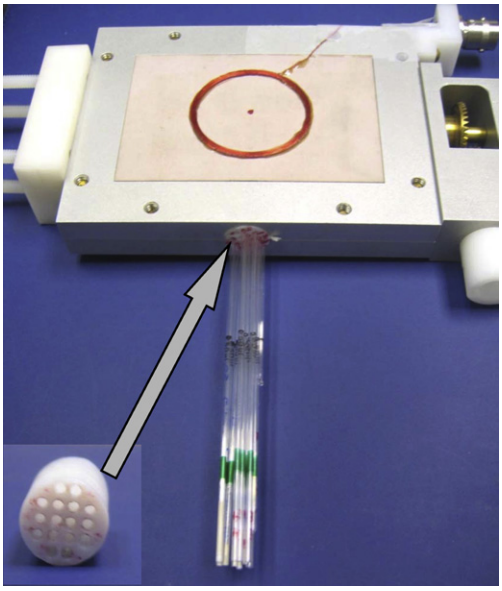

Fig. 6. Experimental setup. A holder with 18 bores is inserted into a 12.6 mm diameter loop-gap resonator. There are total of 17 capillary tubes, each filled with LiNc-BuO up to a height to 5 mm at one end separated by cotton plugs from the varying amount of sodium hydrosulfite at the other end. Each tube was first inserted individually into a specific bore to build the ground truth and then different combinations of tubes were inserted together to collect the composite spectrum.

results are reported in Table 1. Fig. 7 shows results for data set b_3 with 12.4 dB SNR.

4. Discussion

In EPR oximetry, the pO_2 value based on the peak-to-peak (or FWHM) linewidth information is only reliable if the measured signal originates from a single specie with spatially invariant lineshape. For multiple lineshapes, this information can be misleading. A general solution, for such cases, is to perform conventional spectral–spatial imaging. The information from spectral–spatial imaging, although comprehensive, generally requires long acquisition times. Therefore, devising a method to measure an overall pO_2 of a heterogeneous environment can be valuable for clinically relevant scenarios where short acquisition times are a high priority.

In the proposed method, from a single composite lineshape we estimated the linewidth histogram which was then used to compute the mean and median linewidth values. Because the method does not provide any spatial information, it cannot be used to compute hypoxic fraction unless the probe is assumed to be uniformly distributed in the sample or the user has some other relevant a priori information about the spin distribution. The method is flexible enough to accommodate baseline drift and dispersion signal effects that may contaminate the data. The observed results are stable for the range of noise powers considered.

In the first simulation example (Fig. 2), the reconstructed histogram $\hat{x}$ is a good approximation of the original histogram x and so are the mean and median linewidth values. For the second example (Fig. 3), the reconstructed histogram $\hat{x}$ does not match precisely with the input histogram x but mean and median values are still not significantly different. We have observed that for a reasonable estimate of mean and median linewidths, histogram x and $\hat{x}$ need not match precisely. Although a histogram mismatch does seem to result in significant disagreement in high order moments that are not reported here, the calculation of the mean and median linewidth is fairly accurate for realistic noise levels.

Fig. 5 shows results for 50 runs. Using the proposed method, the error mean and standard deviation were 1.7(±44) mG for the estimation of mean linewidth and 11(±83) mG for the estimation of median linewidth. The bias and estimation variance can be further reduced by increasing SNR. Using the apparent linewidth, in comparison, the error and standard deviation were 340(±320) mG for the estimation of mean linewidth and 505(±210) mG for the estimation of median linewidth. Although error is the estimation of the mean and median linewidths is substantially reduced using the suggested method, for biological applications where small changes in mean and median linewidth values carry significance, the attained resolution may not be sufficient especially at low SNR.

Here we are assuming that the selected $[\gamma_{low}, \gamma_{up}]$ closely brackets $[\gamma_{min}, \gamma_{max}]$. However, a precise knowledge of $[\gamma_{min}, \gamma_{max}]$ may not be available in all applications. Therefore, an overly conservative selection for such cases may result in $[\gamma_{low}, \gamma_{up}]$ which is much wider than the actual linewidth range present in the sample. Such extra degrees of freedom may increase estimation bias and standard deviation [19]. However, we have observed that for a moderate increase in $[\gamma_{low}, \gamma_{up}]$ there is no drastic effect on the results. For example, when the selected $[\gamma_{low}, \gamma_{up}]$ is increased from [0.48, 3.20] to [0.30, 3.50] in the simulations, the error bias and standard deviation changed from 1.7(±44) mG to 6.3(±49) mG for the mean linewidth and from 11(±83) mG to 9.6(±98) mG for the median

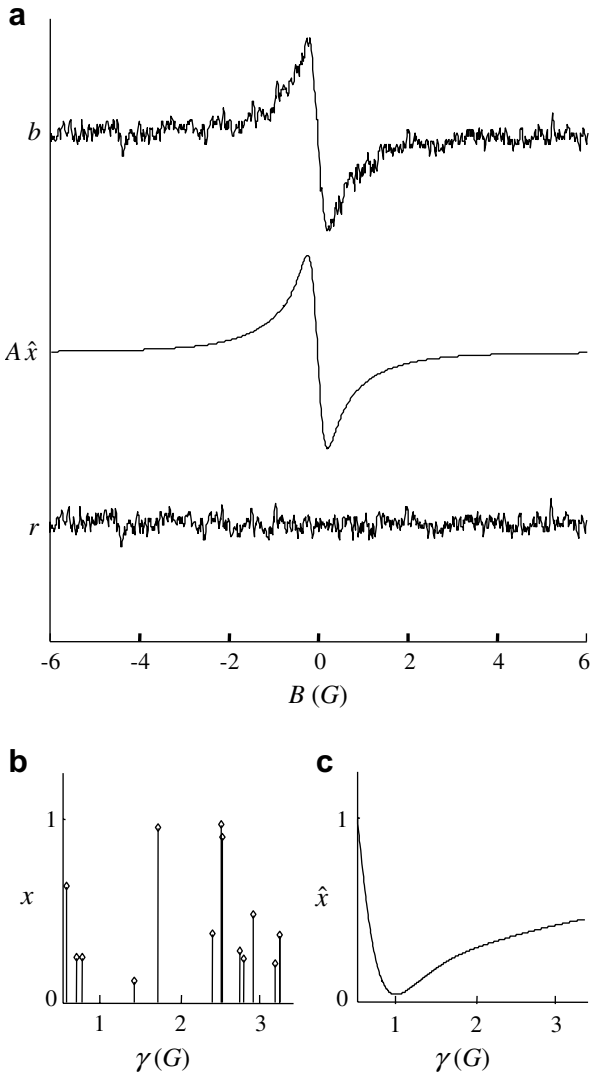

Fig. 7. A example of L-band experiment results. (a) Measured data b, fitting results $A\hat{x}$, and residual r, (b) input histogram x, and (c) estimated histogram $\hat{x}$. Mean linewidths for x and $\hat{x}$ are 2.27 and 2.22 G, while median linewidths for x and $\hat{x}$ are 2.58 and 2.41 G, respectively. Apparent linewidth computed from $A\hat{x}$ is 0.794 G.

Table 1
Results of EPR experiment conducted on an L-band spectrometer

Measurement	SNR (dB)	Apparent linewidth	Input mean	Computed mean	Input median	Computed median
b_1	12.2	0.731	2.23	2.45	2.52	2.71
	24.5	0.732	2.23	2.28	2.52	2.47
b_2	12.3	0.630	1.96	1.89	2.31	2.04
	24.7	0.651	1.96	2.04	2.31	2.28
b_3	12.4	0.794	2.27	2.22	2.58	2.41
	24.0	0.751	2.27	2.24	2.58	2.43

Three different composite spectra were generated by three different combinations of capillary tubes, filled with LiNc-BuO and varying amounts of Na_2SO_3, each having its own linewidth and spin density. For each spectrum two different SNRs are considered. All values are in G.

linewidth. However, selecting a $[\gamma_{low}, \gamma_{up}]$ that is much wider than $[\gamma_{min}, \gamma_{max}]$ may introduce significant errors for low SNR data.

For a heterogeneous pO_2 environment, such as a tumor, the peak-to-peak value of the lineshape is biased towards narrow lineshapes. On the other hand, the mean and median pO_2 values computed using this method are better representations of overall sample oxygenation. However, the effectiveness of a single pO_2 number, as compared to spectral–spatial imaging, in a clinically relevant model requires further investigation. The more informative description provided by spectral–spatial imaging is obtained at the cost of acquisition time. Our experimental results also match our simulations for a wide range of SNR. This method is computationally fast and does not require special computing resources. For example, it takes Matlab (Natick, MA) less than a minute to run 2500 iterations on a Pentium 4 processor with 1 GB RAM.

5. Conclusion

For a heterogeneous environment, the pO_2 estimation based on peak-to-peak signal amplitude can be misleading because components with smaller linewidth have more impact on the overall peak-to-peak linewidth. A reliable estimate of the mean and median pO_2 can be obtained by recovering the underlying linewidth histogram. We have implemented and tested a postprocessing method to estimate the linewidth histogram and extract the mean and median pO_2.

Acknowledgments

We thank Sergey Petryakov for technical assistance. This work was funded by NIH Grant EB005004.

References

[1] H.J. Halpern, C. Yu, M. Peric, E. Barth, D.J. Grdina, B.A. Teicher, Oximetry deep in tissues with low-frequency electron paramagnetic resonance, Proc. Natl. Acad. Sci. USA 91 (1994) 13047–13051.
[2] W.K. Subczynski, S. Lukiewicz, J.S. Hyde, Murine in vivo L-band ESR spin-label oximetry with a loop-gap resonator, Magn. Reson. Med. 3 (1986) 747–754.
[3] J.L. Zweier, S.T. Gorman, P. Kuppusamy, Measurement of oxygen concentrations in the intact beating heart using electron paramagnetic resonance spectroscopy: a technique for measuring oxygen concentrations in situ, J. Bioenerg. Biomembr. 23 (1991) 855–871.
[4] H.M. Swartz, T. Walczak, Developing in vivo EPR oximetry for clinical use, Adv. Exp. Med. Biol. 454 (1998) 243–252.
[5] A. O'Hara, F. Goda, J.F. Dunn, H.M. Swartz, Potential for EPR oximetry to guide treatment planning for tumors, Adv. Exp. Med. Biol. 411 (1997) 233–242.
[6] R.A. Kloner, R.B. Jennings, Consequences of brief ischemia: stunning, preconditioning, and their clinical implications: part 1, Circulation 104 (2001) 2981–2989.
[7] K.J. Liu, P. Gast, M. Moussavi, S.W. Norby, N. Vahidi, T. Walczak, M. Wu, H.M. Swartz, Lithium phthalocyanine: a probe for electron paramagnetic resonance oximetry in viable biological systems, Proc. Natl. Acad. Sci. USA 90 (1993) 5438–5442.
[8] M.M. Maltempo, S.S. Eaton, G.R. Eaton, Spectral–spatial two-dimensional EPR imaging, J. Magn. Reson. 72 (1987) 449–455.
[9] O.Y. Grinberg, A.I. Smirnov, H.M. Swartz, High spatial resolution multi-site EPR oximetry: the use of a convolution-based fitting method, J. Magn. Reson. 152 (2001) 247–258.
[10] B.B. Williams, O.Y. Grinberg, E. Demidenko, H.M. Swartz, Resolution of heterogeneity of oxygen in tissues using EPR oximetry with particulates, Proc. Int. Soc. Magn. Reson. Med. 11 (2004) 2256.
[11] B. Eicke, Iteration methods for convexly constrained ill-posed problems in Hilbert space, Numer. Funct. Anal. Opt. 13 (1992) 413–429.
[12] A.N. Tikhonov, V.A. Arsenin, Solution of Ill-Posed Problems, Winston & Sons, Washington, 1977.
[13] A. Sabharwal, L.C. Potter, Convexly constrained linear inverse problems: iterative least-squares and regularization, IEEE Trans. Signal Process. 46 (1998) 2345–2352.
[14] P.C. Hansen, Rank-Deficient and Discrete Ill-Posed Problems, SIAM, Philadelphia, 1998.
[15] P. Tan, C. Drossos, Invariance properties of maximum likelihood estimators, Math. Mag. 48 (1975) 37–41.
[16] B.L. Bales, M. Peric, M.T. Lamy-Freund, Contributions to the gaussian line broadening of the proxyl spin probe EPR spectrum due to magnetic-field modulation and unresolved proton hyperfine structure, J. Magn. Reson. 132 (1998) 279–286.
[17] R.P. Pandian, N.L. Parinandi, G. Ilangovan, J.L. Zweier, P. Kuppusamy, Novel particulate spin probe for targeted determination of oxygen in cells and tissues, Free Radic. Biol. Med. 35 (2003) 1138–1148.
[18] M.F. Yu, I. Gorenne, X. Su, R.S. Moreland, M.I. Kotlikoff, Sodium hydrosulfite contractions of smooth muscle are calcium and myosin phosphorylation independent, Am. J. Physio. 275 (1998) 976–982.
[19] A. Walden, Variance and degrees of freedom of a spectral estimator following data tapering and spectral smoothing, Signal Process. 20 (1990) 67–69.
[20] S. Som, L.C. Potter, R. Ahmad, P. Kuppusamy, A parametric approach to spectral–spatial EPR imaging, J. Magn. Reson. 186 (2007) 1–10.